Low-noise and compact detection system using RF MEMS switch for solid-state NMR spectroscopy at cryogenic temperature: proof-of-concept experiment

Sotaro Nishioka[1,2†], Naoki Sakuyama[2], Ken Obara[3,4], Akiko T. Saito[1], Mitsuharu Yashima[2], Hidekazu Mukuda[2]

[1]*National Institute for Materials Science, Ibaraki 305-0003, Japan*
[2]*Graduate School of Engineering Science, Osaka University, Toyonaka, Osaka 560-8531, Japan*
[3]*Graduate School of science, Osaka Metropolitan University, Osaka 558-8585, Japan*
[4]*Equipment Sharing Center for Advanced Research and Innovation (ESCARI), Osaka Metropolitan University, Osaka 558-8585, Japan*

Keywords: NMR, MEMS switch, Cryogenic amplifier, HEMT, Cryogenics

†Present affiliation: *Faculty of Engineering, Niigata University, Niigata 950-2181, Japan*

Abstract

In nuclear magnetic resonance (NMR) spectroscopy, the signal from nuclear spins is extremely weak, and thus it has been desired to improve the signal-to-noise ratio (SNR). In this study, we designed a compact low-noise probe and peripheral detection system optimized for low-temperature solid-state NMR spectroscopy. We confirmed the operation of a Tx/Rx switch composed of radio frequency microelectromechanical system (RF MEMS) switches and a preamplifier using high electron mobility transistors (HEMT), which can operate even at 20 K and under a high magnetic field of approximately 10 T. In our compactly designed NMR system, we succeeded in sufficiently reducing both thermal noise and external noise. As a result, the ^{195}Pt- and ^{27}Al-NMR measurements for Pt and Al solid powder samples were performed at 12 T and down to 20 K, showing that the SNR was improved by 40 - 50% compared with the conventional system. These experiments also provide information on the low temperature properties and operational characteristics of integrated RF electronic devices, such as the RF MEMS switch, the HEMT, and their combined circuit system.

1. Introduction

Nuclear magnetic resonance (NMR) spectroscopy is a technique that uses the resonance phenomenon of nuclear spins with a high-frequency electromagnetic field to investigate the properties of materials. Since it is a non-destructive and non-invasive method, it is widely used in a variety of practical applications, such as the determination of organic structures and complex mixtures and medical imaging by magnetic resonance imaging (MRI). In low-temperature physics research, solid-state NMR spectroscopy is an indispensable method that provides a microscopic view of the physical properties of novel materials. However, the NMR signal intensity of solids is extremely low due to the large broadening of the spectra compared with liquid-state NMR in general. Therefore, to reduce the measurement time and perform the fine analyses, it has been desired to increase the SNR, *i.e.*, to increase the signal and decrease various noises at the same time. Especially in the cases of minute solid samples, various attempts to improve the SNR have been reported [1-8]; for example, the use of meander or spiral coil for the thin film samples [1,2] and Lenz lens coil for micrometer-sized samples in the high-pressure cell [3-6], which made the detection of the small NMR signals more efficient by increasing the effective filling factor even for the minute solid samples. Moreover, MEMS capacitors can improve the Q factor of the resonant circuit [9,10].

Furthermore, in order to improve the SNR, it is necessary to reduce the noise. The detection system around the NMR probe consists of a resonant circuit with a detection coil, a preamplifier, a duplexer, and coaxial cables connecting them (see Fig. 1(b)). For high-frequency experiments, electromagnetic shielding with metals is a basic technique. Solid-state NMR in low-temperature physics is typically performed in a metal dewar with an integrated superconducting magnet filled with liquid helium (He). The sample space of the cryostat in the magnet is typically tens of millimeters in diameter, so the preamplifier and duplexer are usually placed outside the dewar at room temperature. Since the cable length between the detection coil and the preamplifier is typically a few meters or more, there is a possibility of noise intrusion from the cable which also acts as an antenna. Furthermore, it is also important to reduce the Johnson-Nyquist noise, *i.e.* thermal noise from the devices located at high temperatures. Therefore, cooling the detection coil and the amplifier is an effective method, which has been developed as a cryoprobe [11-19]. Recently, the techniques of cryoprobe and magic angle spinning (MAS) are combined to improve SNR and spectral resolution [17,19]. In fields such as astrophysics and quantum computing, the amplifiers optimized for each purpose using high electron mobility transistors (HEMT) operating at cryogenic temperatures, have been used to increase sensitivity [20,21]. In general, the noise figure (NF) of preamplifiers decreases with decreasing temperature, since the thermal noise power is proportional to temperature. As for low-temperature physics, a sample is typically cooled to cryogenic temperatures below 80 K. Further low-temperature NMR study has been performed below 1 K using a dilution refrigerator. Therefore, it is reasonable to integrate the detection coil, preamplifier, and all connecting lines inside the probe in the cryogenic part and separate them from the room temperature part [17,18]. Such an NMR system is enclosed in a metal dewar, and is therefore expected not only to reduce Johnson-Nyquist noise but also to be robust against various external noises from the environment. Recently, it was effectively applied to electron paramagnetic resonance [22].

To realize such a compact system, the duplexer must also be placed between the detection coil and the preamplifier at

cryogenic temperatures. The duplexer is a device that allows transmission of radio frequency (RF) pulses and reception of RF signals and acts as a switch between the transmitter and receiver in the spectrometer. However, it is challenging to downsize and operate a duplexer at low temperatures since it generally consists of λ/4 lines and silicon diodes. Therefore, in this study, we attempted to use RF microelectromechanical system (MEMS) switches as a switch that actively operates in the broadband, instead of a duplexer. So far, there are no reports of MEMS switches that can operate at temperatures below 43 K [18,23-25]; however, they have promising features such as a relatively small size on the order of millimeters and high-speed switching time of 10 - 100 μs.

In this paper, we report the development of an original compact probe that integrates a preamplifier using HEMT and a Tx/Rx switch consisting of two RF MEMS switches near the detection coil. We confirmed the operation of the HEMT preamplifier at a cryogenic temperature of 4.2 K under a high magnetic field of about 10 T. The RF MEMS switch operated from 20 to 300 K under a magnetic field of ~10 T. The original NMR probe, which includes the preamplifier and the Tx/Rx switch integrated near the sample, successfully operated down to 20 K at 12 T. As a result, we succeeded in performing solid-state NMR measurements in ^{27}Al and ^{195}Pt metal samples down to 20 K at 12 T, and showed the apparent reduction of noise. The improvement in SNR of our original system was achieved by 40 - 50% at 20 K compared with the conventional NMR system.

2. Experiments

2.1 Concept of whole design of improved NMR probe and transmission/reception system

Figure 1(a) shows a schematic diagram of the transmission/reception system in our improved NMR probe, including the RF MEMS switch and the cryogenic preamplifier. There are four coaxial cables with an impedance of 50 Ω connecting to the probe from outside at room temperature, which are two control cables for two RF MEMS switches, a transmission cable for the RF pulse, and a reception cable to detect the NMR spin-echo signal. Although it is usually placed outside the dewar in the conventional system (see Fig. 1(b) for comparison), the preamplifier is placed inside the probe to reduce the noise in the present system. Instead of the duplexer in conventional system, the Tx/Rx switch, which consists of two RF MEMS switches, is placed between the amplifier and the detection coil, as shown in Fig. 2. Here, switches 1 and 2 are located at the inlet end and the preamplifier end, respectively (see Fig. 1(a)). When the RF pulse is applied to excite the nuclear spins, switch 1 at the inlet end is set to "ON" to pass the RF pulse. At the same time, switch 2 at the preamplifier end is set to "OFF" to protect the preamplifier from the high-power RF pulse. After excitation by the RF pulse, switch 2 is set to "ON" to detect the spin echo signal through the preamplifier. At this time, switch 1 is set to "OFF" to protect the spin echo signal from noise through the inlet line. This system is enabled by the high-speed operation (~10 μs) and high-power handling (150 W) of the RF MEMS switch (MM5130; Menlo Micro). The device contains four individual switches, which are connected in parallel to reduce contact resistance (< 1 Ω at room temperature). Considering that the input impedance of the amplifier is 50 Ω, the signal attenuation caused by the MEMS switch is less than 2%. In "OFF" state, the isolation of switch circuit is -45 dB at 100 MHz at room temperature. Additionally, the package only contains cantilever structure contacts and does not contain any power supply circuit using semiconductor components to operate the switches. Therefore, it is possible to operate the device at cryogenic temperatures, and a high voltage signal of 89 V needs to be applied to control the switches. Moreover, since the RF MEMS switch operates at frequencies from DC to 26 GHz, the Tx/Rx switch based on this approach also operates over a wide frequency range.

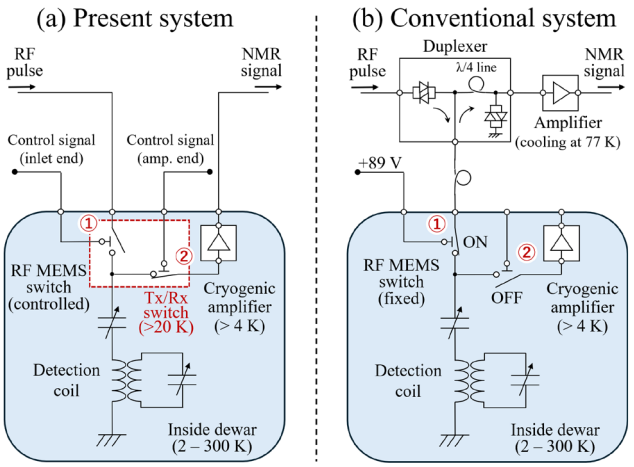

Fig. 1 (a) Schematic diagram of the present NMR system using RF MEMS switches and an internal cryogenic amplifier. (b) Schematic diagram of the conventional NMR system with a duplexer and an external amplifier for comparison. By setting switch 1 to a fixed "ON" and switch 2 to a fixed "OFF", the present system (a) can be easily switched and compared with the conventional system (b) using the same probe for comparison.

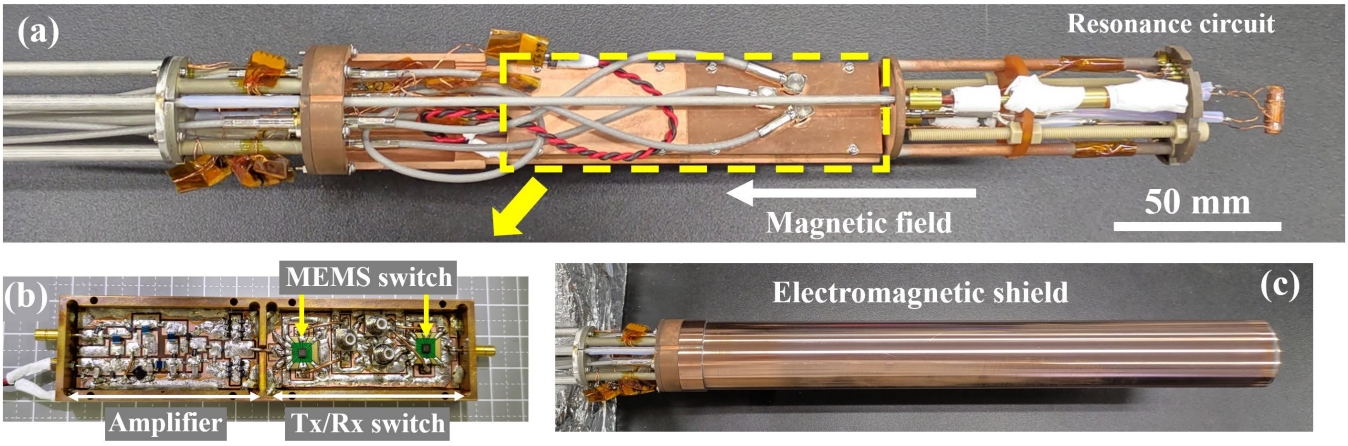

Fig. 2 Photograph of (a) the probe, (b) the amplifier and the Tx/Rx switch using the RF MEMS switches integrated into the probe, and (c) the probe covered with the electromagnetic shield. A magnetic field was applied along the probe, parallel to the substrates of the RF MEMS switches in the Tx/Rx switch and the HEMT in the amplifier. The magnetic field was about 10 T at the position near the amplifier when the field was set to 12 T at the sample position. The temperature inside the dewar is monitored by two thermometers at the sample in the detection coil and the amplifier position.

Figure 3 shows the control procedure of two RF MEMS switches. The control signals for both switches were supplied by boosting the synchronized control signal with the RF pulse from the pulse control equipment to 89 V. Since both switches operate in an anti-phase mode, an inverting circuit is used for the switch at the amplifier end. The switching operation time must be shorter than the time between the end of the π pulse and the beginning of the spin echo, as shown in Fig. 3. In order to prevent hot switching, which causes the switch to break down, the voltage change of the control signal must occur before the RF pulse and after the RF pulse. As shown in Fig. 2(a), the preamplifier was placed 200 mm above the detection coil including the sample placed at the center of the magnetic field.

Here, we compared the SNR of the conventional system (Fig. 1(b)) with that of the present system (Fig. 1(a)) to evaluate the effectiveness of the present system. The external amplifier in the conventional system (LNA-4R3; Sankyodensei Corp.) achieves an NF of less than 0.5 dB at ~100 MHz. To compare the two systems, the present system can be switched and compared with the conventional system using the same probe, as shown in Fig. 1(b), by setting switch 1 to a fixed "ON" and switch 2 to a fixed "OFF". This approach allows the Q factor (~80) setting of the resonance circuit to be shared between the two systems. The temperature inside the dewar was monitored by thermometers (Cernox CX-1050-AA) at both the sample and the amplifier chassis positions. The temperatures at these positions differed slightly: typically, when the sample temperatures were fixed at 77 K and 20 K, the temperatures at the amplifier were 84 K and 23.5 K, respectively. This can be attributed to two possible causes: one is heat intrusion from the four coaxial cables. The other is the heat generation by the amplifier (see section 2.2). The magnetic field was evaluated from the resonance frequency of a ^{27}Al-NMR signal, which was 12 T at the sample position at the magnet center, and about 10 T at the amplifier position. Note that the field was applied along the direction parallel to the substrates of the RF MEMS switch and the HEMT.

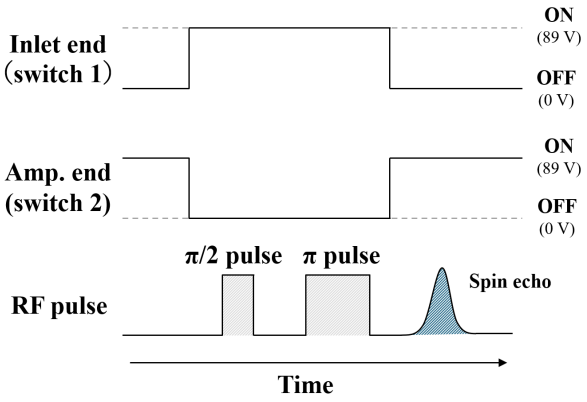

Fig. 3 Control procedure of RF MEMS switches and RF pulse. The switching time must be shorter than the time between the end of the π pulse and the beginning of the spin echo. To avoid hot switching, which can cause breakdown, the voltage change of the control signal must occur before the RF pulse and after the RF pulse. The control signals for both switches are synchronized with the RF pulse sequence.

2.2 Design of cryogenic pre-amplifier

The compact amplifier is built into the present NMR probe, as shown in Fig. 2(b). Its performance was examined down to cryogenic temperatures under a high magnetic field. Figure 4(a) shows the circuit diagram of the amplifier using enhancement mode pseudomorphic high electron mobility transistors (E-pHEMT) (SAV-551+; Mini-Circuits). Here, we have selected the electronic components that are empirically known to operate at cryogenic temperatures, such as thin-film resistors, air-core inductors, tantalum capacitors, multilayer ceramic capacitors (with small temperature coefficients, such as C0G), and Schottky barrier diodes [20]. The gain of the amplifier was maintained above 30 dB across a wide frequency range from 10 MHz to 200 MHz, and it remained operation over the wide temperature range from 300 K to 4.2 K. Here, the optimum supply voltage (current) increased from 0.7 V (20 mA) to 1.2 V (50 mA) as the temperature decreased from 300 K to 4.2 K. As

shown in Fig. 4(b), we confirmed that the gain remained above 30 dB even at 4.2 K under ~10 T. The inset of Fig. 4(b) shows the experimental result of a 100 MHz sinusoidal signal amplified by this amplifier, indicating that it maintains an ideal sinusoidal waveform. Note that the amplifier itself was able to operate even at a cryogenic temperature of 4.2 K and under a high magnetic field of ~10 T. The NF of the amplifier was estimated by the gain method (direct method) using the equation below,

$$NF = 10\log_{10}\left(10^{\frac{P_{NOUT}}{10}} - 10^{\frac{P_{floor}}{10}}\right) - (P_j + G),$$

where P_{NOUT} is the observed noise power, P_{floor} is the noise floor of spectrum analyzer, P_j is the power of Johnson-Nyquist noise, and G is the amplifier gain. In this case, we obtained these parameters, P_{NOUT} = -136.1 dBm/Hz, P_{floor} = -153.0 dBm/Hz, P_j = -173.9 dBm/Hz at 298 K and G = 35.7 dB at room temperature and 100 MHz, and thus NF = 2.0 dB is estimated at 100 MHz.

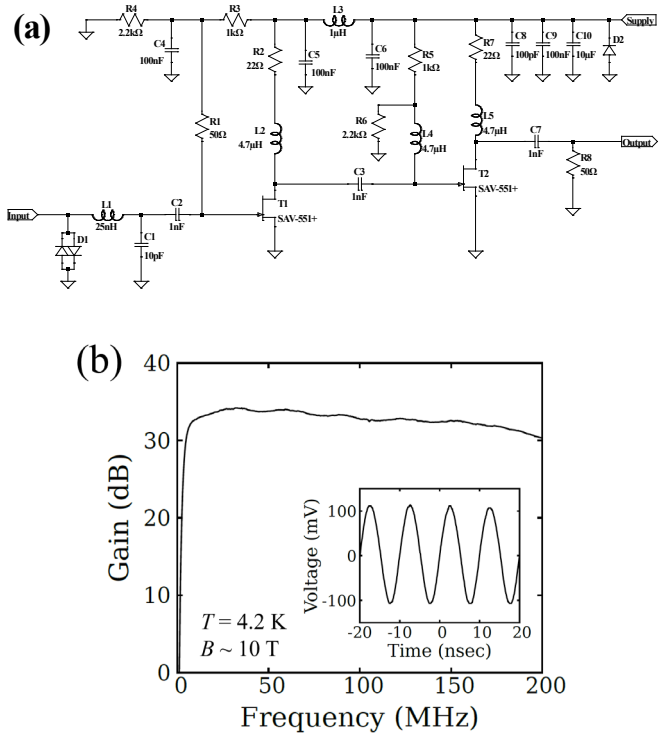

Fig. 4 (a) Amplifier circuit using E-pHEMT. An optimum supply voltage increased from 0.7 V (20 mA) to 1.2 V (50 mA) with a decreasing temperature from 300 K to 4.2 K. (b) Frequency dependence of the gain under a magnetic field of ~10 T at 4.2 K, showing that the gain remains above 30 dB over a wide frequency range from 10 to 200 MHz. The inset shows an amplified sine wave at 100 MHz, indicating that it maintains an ideal sinusoidal shape even at low temperatures down to 4.2 K and under a high magnetic field of ~10 T.

Figure 5 shows the equivalent input noise (EIN) of the amplifier at each amplifier temperature under a magnetic field of ~10 T, which was obtained by dividing the measured noise by the gain of the amplifier. The results indicate that the noise level is successfully reduced with decreasing temperature. The voltage of Johnson-Nyquist noise is independent of frequency up to terahertz region and proportional to the square root of temperature. It is given by $V_n = \sqrt{4k_B TRB}$, where k_B is the Boltzmann constant, R is a resistance, and B is a bandwidth. The ratio of the noise level at each temperature can be approximately explained by the ratio of the square roots of those temperatures, indicating that the Johnson-Nyquist noise is reduced by cooling the amplifier, as expected. On the other hand, the existence of frequency dependence in the spectra also point out the presence of other noise, such as external noise.

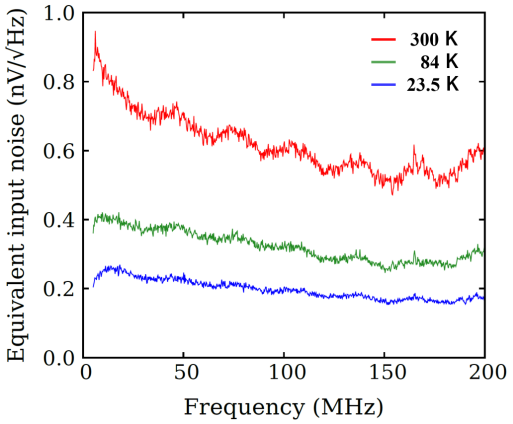

Fig. 5 Equivalent input noise of the amplifier at each amplifier temperature under a magnetic field of ~10 T. The noise level is reduced with decreasing temperature.

2.3 Operation test of RF MEMS switch

A preliminary operation test of the RF MEMS switch was performed under a high magnetic field of ~10 T over a wide temperature range from 300 K to 4.2 K, using the test circuit shown in Fig. 6(b). A DC voltage of 5 V was applied between the terminals of the RF MEMS switch for the test, and the RF MEMS switch was controlled by the control signal with a pulse duration of 30 μs. Figure 6(a) shows the results of the time variation of voltage at various temperatures. When the temperatures were higher than 77 K, the typical duration from "OFF" to "ON" required ~10 μs, and the opposite duration from "ON" to "OFF" required ~2 μs typically. They were consistent with the datasheet of this device. However, at 20 K, when the switch was turned from "ON" to "OFF", chattering of the cantilever unexpectedly occurred for a pulse width of less than 1 μs, with a period of about 8 μs and a duration of no more than 85 μs, as shown in Fig. 6(a), although the duration from "OFF" to "ON" was the same as that in the datasheet. This behavior introduces a small amount of noise intrusion. When it was cooled down to 4.2 K, the RF MEMS switch froze and stopped working; however, the switch restarted when the temperature was raised above 20 K. Therefore, the NMR measurements were performed above 20 K in this study.

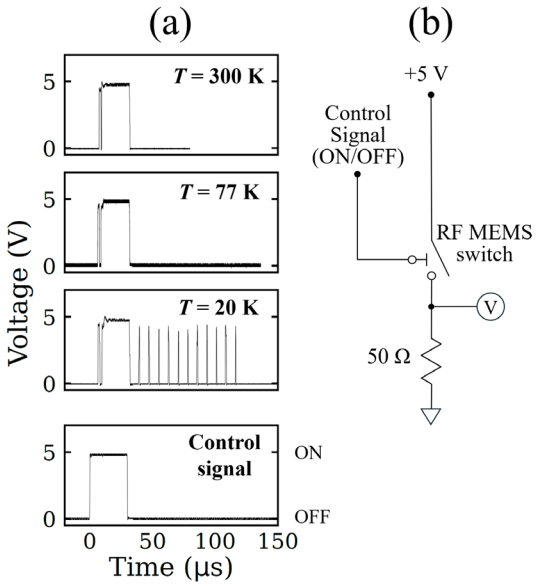

Fig. 6 (a) Result of an operation test of the RF MEMS switch at 300 K, 77 K and 20 K under a magnetic field of ~10 T. (b) Circuit diagram used for this test. At 300 K and 77 K, the response speed is consistent with the device datasheet. However, chattering occurred when turning off at 20 K.

3. Results and Discussion

3.1 NMR measurement for Pt and Al metals

As shown in Figs. 1(a) and 2, we compactly integrated two RF MEMS switches and the preamplifier inside the probe, and performed ^{195}Pt- and ^{27}Al-NMR measurements using our improved NMR system. Figure 7 shows the ^{195}Pt-NMR spectrum for the Pt powder sample measured under 12 T at 20 K. The Knight shift is approximately -4%, which is consistent with the value reported previously [26-28]. The linewidth is FWHM = 105 ppm. A gyromagnetic ratio of γ_n = 9.094 MHz/T for ^{195}Pt was used.

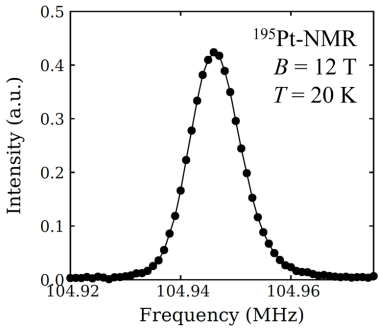

Fig. 7 ^{195}Pt-NMR spectrum of a Pt powder sample observed with the present system under 12 T at 20 K.

We discuss the SNR of the present system compared with that of the conventional system. To obtain the SNR, the noise level was evaluated by analyzing the noise normalized by the voltage of an appropriately averaged spin echo peak. Figure 8(b) shows an example of the single-shot NMR signal with noise for the present system and the conventional system before accumulation. After sufficient accumulation, the spin echo signal was observed at around t = 200 μs. To evaluate the background noise, the normalized signal was analyzed to obtain a histogram using the data from 400 to 1600 μs where there is no spin echo signal. Figure 8(c) shows the standard deviation σ for the noise in both the present and conventional systems, obtained by fitting the histogram with the Gaussian distribution. In fact, the histogram of the present system exhibits a narrower distribution compared with that of the conventional system as shown in Fig. 8(c). The σ values of the present and conventional systems are σ_p = 0.806 and σ_c = 1.206, respectively; therefore, we evaluated the σ ratio of the present and conventional systems, namely, the relative SNR gain to be σ_c/σ_p = 1.50 at 20 K, indicating that the noise was suppressed in the present system. The 50% increase in SNR means that, since noise decreases with the square root of the number of acquisitions, the data with the same quality can be obtained effectively in only nearly half (~1/2.25) of the original measurement time.

Figure 8(a) shows the relative SNR gain of the present system compared with that of the conventional system measured by ^{195}Pt-NMR in the temperature range from 20 to 300 K. Since the results for the two systems are compared at the same sample and detection coil temperatures, the effects of the Boltzmann distribution among energy levels of nuclear spins and of noise reduction by cooling the detection coil can be excluded. The ratios exceed 1.0 below ~77 K, indicating that the SNR of the present system was largely improved compared with that of the conventional system below ~77 K. Note that the ratio does not exceed 1.0 at 300 K. This may be due to the fact that the NF of the developed amplifier is 1.5 dB larger than that of the external amplifier, which corresponds to a noise increase of 19%.

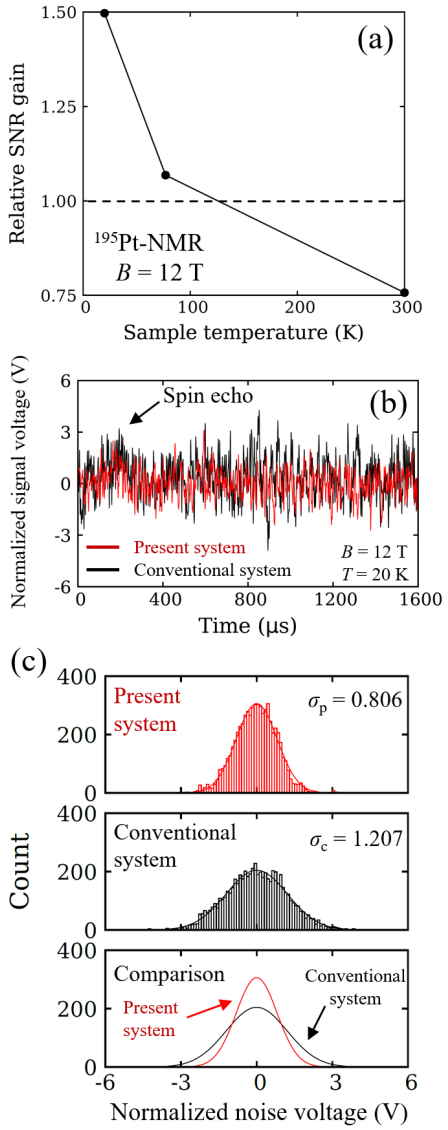

Fig. 8 (a) Relative SNR gain of the present system compared with the conventional system at each temperature, as evaluated by ^{195}Pt-NMR in the Pt powder sample. (b) Single-shot NMR signal with noise at 20 K normalized by the voltage of the appropriately averaged ^{195}Pt spin echo peaks. (c) Histogram made by the background noise data from 400 to 1600 μs of Fig. 8(b). The standard deviation σ for the noise was evaluated by fitting the histograms with Gaussian distribution for the present system (top), the conventional systems (middle). The bottom figure shows a comparison of their fitting curves. The histogram of the present system exhibits a narrower distribution than that of the conventional system, indicating that the noise is reduced.

For comparison, we also performed a ^{27}Al-NMR measurement in the Al powder sample at 12 T. Figure 9 shows the relative SNR gain of the present system over the conventional system for ^{27}Al-NMR at each temperature. The relative SNR gain of the ^{27}Al-NMR measurement also increased with decreasing temperature, indicating the same trend observed in ^{195}Pt-NMR measurement. We evaluated the relative SNR gain to be $\sigma_c/\sigma_p = 1.40$ at 20 K. As a result, the SNR for Al samples as well as the Pt samples was improved by more than 40% compared with the conventional system at 20 K. We note that, if we could prevent the RF MEMS switch from freezing and chattering below 20 K, we could expect that the SNR is improved by larger than 40 - 50%.

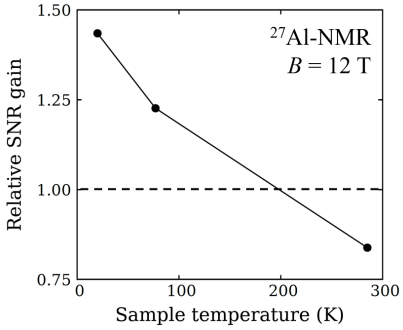

Fig. 9 Relative SNR gain of the present system compared with the conventional system at each temperature for ^{27}Al-NMR under 12 T. The SNR for Al samples were improved by more than 40% compared with the conventional system at 20 K.

3.2 Noise measurement

To investigate the reasons for the SNR improvement by the present system, the noise spectra of the present and conventional systems were measured using the spectrum analyzer. Figures 10(a) - 10(c) show the EIN spectra passed through the internal amplifier in the present probe at various detection coil temperatures (Fig. 1(a)). Here, the resonance circuit was tuned to the resonance frequency at 105 MHz for ^{195}Pt under 12 T, as indicated by the arrows in Fig. 10 and Fig. 11. These measurements were performed at different temperatures under three settings of the two switches shown in the right panel of Figs. 10(a) - 10(c). These EIN spectra were obtained simply by dividing the measured noise by the gain of the amplifier to exclude the frequency dependent of the gain, and they still contain noise from various sources.

First, both switches were set to “ON” position (Fig. 10(a) right). As shown in Fig. 10(a), many peaks were found in the noise spectra. We confirmed that almost all the peaks in the figure correspond to the external noise outside the dewar intruding from the RF pulse cable for the following two reasons: (1) they disappeared when the switch at the inlet end was "OFF" (Fig. 10(b)), and (2) they were independent of the temperature of the detection coil and the amplifier. However, the peaks at the tuning frequency of 105 MHz still remain even when the switch at the inlet end was "OFF" (Fig. 10(b)), indicating that the resonance circuit is still detecting the noise sensitively due to its low impedance. Note that the comparison of the absolute values of noise among the three modes is not reasonable, because the lengths and temperatures of cables connected in each mode are different. When detecting the spin echo signal in the present system (Fig. 1(a)), the switch modes are set to the positions in Fig. 10(b). Lastly, both switches were set to “OFF” position (Fig. 10(c)). The presence of attenuated noise that intruded and/or bypassed the switch was also observed, even when these switches were not connected to either end. The reductions in the noise level with decreasing the detection coil temperature were observed in Figs. 10(b) and 10(c), which correspond to the measurement results of the EIN of the amplifier shown in Fig. 5. In other words, to maximize amplifier performance, it is necessary to suppress the noise that intrudes the detection system. The overall results suggest that the switch provides significant noise reduction. Furthermore, there is room for improvement in

countermeasures against noise from external sources other than the RF pulse cable, such as ground. On the other hand, the noise peaks around 180 MHz were observed at all temperatures and under all switch positions, suggesting that the noises around 180 MHz intrude from the vicinity of the amplifier; however, they do not disturb the detection of NMR signal because those frequencies are largely different from the resonant frequencies of ^{195}Pt and ^{27}Al.

Figure 11 shows the EIN passing through the external amplifier in the conventional system (Fig. 1(b)) at various temperatures. There are many peaks independent of temperature, indicating that they originate from external noise outside the dewar. It is speculated that the noise in the present system is suppressed over various frequencies, as seen in Fig. 10(b), due to disconnection of the RF pulse inlet line and the cooling of the system. It may lead to the improvement in the SNR compared with the conventional system.

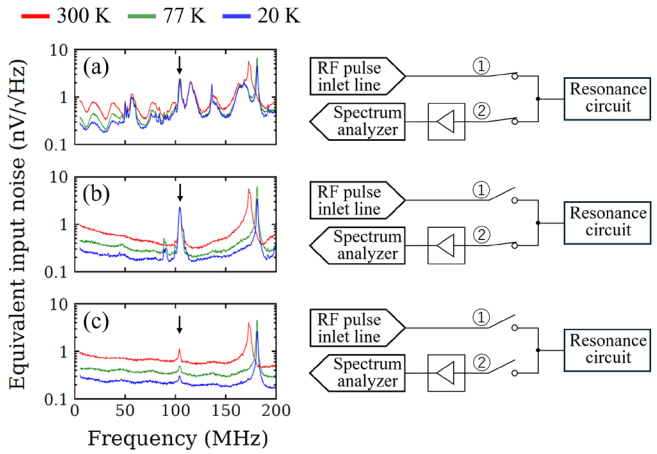

Fig. 10 Equivalent input noise spectra of the present system at various detection coil temperatures, which are measured under three settings of the two switches (right panels). The results when (a) both switches are initially set to "ON" position, when (b) the switch at the inlet end is set to "OFF", while the switch at the amplifier end is set to "ON" position, and (c) both switches are set to "OFF". The detection of the spin echo signal is performed on the switch position of (b) in the present system. Arrows show the resonance frequency of the resonance circuit.

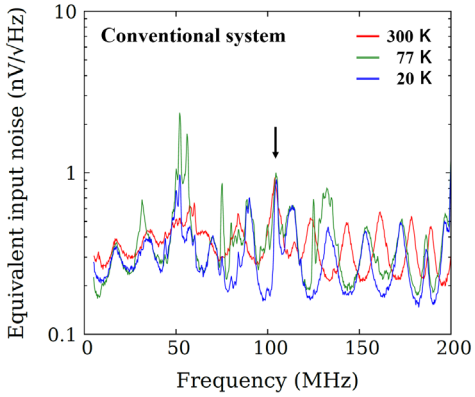

Fig. 11 Equivalent noise spectra of the conventional system at various temperatures. Arrow shows the resonance frequency of the resonance circuit. Noise peaks are independent of temperature, indicating that the conventional system is disturbed by external noise outside the dewar.

4. Summary

We developed the NMR probe with the compact low-noise detection system optimized for low-temperature solid-state NMR spectroscopy. In order to decrease both Johnson-Nyquist noise and external noise, the system includes both the Tx/Rx switch consisting of RF MEMS switches and the HEMT preamplifier in the probe where the detection coil is positioned adjacent to these components. The performance of the present NMR probe, the HEMT amplifier and RF MEMS switch were investigated under a high magnetic field at various temperatures. The HEMT amplifier was operated even under a high magnetic field of ~10 T at a cryogenic temperature of 4.2 K, achieving a gain of over 30 dB. The RF MEMS switch was operated under ~10 T down to 20 K. The NMR measurements for ^{195}Pt and ^{27}Al powder samples using the present NMR system were successful from 20 K to 300 K under a high magnetic field of ~12 T. As a result of a large reduction in both Johnson-Nyquist noise and external noise, the SNRs in ^{195}Pt- and ^{27}Al-NMR measurements were improved by 50% and 40%, respectively, compared with the conventional system at 20 K. In other words, the data with the same quality can be achieved in about half of the original measurement time. This technique is expected to bring greater progresses when it is combined with other techniques, such as planar coils, MEMS capacitors, and MAS. Moreover, the result indicates that a larger SNR can be achieved at lower temperatures, if the chattering of the RF MEMS switch at about 20 K and freezing below 20 K can be prevented. Unfortunately, these issues impose the minimum temperature limit on the present NMR measurement system. Furthermore, the noise spectrum measurements demonstrate that the Tx/Rx switch in the present system reduced noise; however, there is still room for improvement in countermeasures against noise by electromagnetic shielding, and thus further improvements in SNR are expected.

These results provide basic information on the low temperature properties and operational characteristics of the RF MEMS switch and the HEMT. The proof-of-concept of the compact low-noise detection system for NMR was proposed toward future applications in low-temperature solid-state NMR spectroscopy.

Acknowledgement

The authors acknowledge Grants-in-Aid for Scientific Research from Japan Society for the Promotion of Science (JSPS KAKENHI Grant Number JP23H00550 and JP25K00959). This work was partly supported by Izumi science and technology foundation, Casio science promotion foundation, Takahashi Industrial and Economic Research Foundation, Nippon Sheet Glass Foundation, and Yamaguchi Educational and Scholarship Foundation.

Author declarations

The authors have no conflicts to disclose.

Reference

[1] Y. Ishikawa, Y. Koizumi, Y. Fujii, T. Oida, A. Fukuda, S. Lee, E. Kobayashi, H. Kikuchi, J. Järvinen, S. Vasiliev, and S. Mitsudo, “Millimeter-Wave Band Resonator with Surface Coil for DNP–NMR Measurements”, *Appl. Mag. Reason.* **52**, 317-335 (2021). https://doi.org/10.1007/s00723-021-01328-z

[2] W. Liu, L. Lu, and V. F. Mitrovic, “Application of surface coil in nuclear magnetic resonance studies of physical properties of quasi-2D materials”, *Rev. Sci. Instrum.* **88**, 113902 (2017). https://doi.org/10.1063/1.4986047

[3] T. Meier, N. Wang, D. Mager, J. G. Korvink, S. Petitgirard, and L. Dubrovinsky, “Magnetic flux tailoring through Lenz lenses for ultrasmall samples: A new pathway to high-pressure nuclear magnetic resonance”, *Sci. Adv.* **3**, eaao5242 (2017). https://doi.org/10.1126/sciadv.aao5242

[4] J. Schoenmaker, K. R. Pirota, and J. C. Teixeira, “Magnetic flux amplification by Lenz lenses”, *Rev. Sci. instrum.* **84**, 085120 (2013). http://dx.doi.org/10.1063/1.4819234

[5] N. Spengler, P. T. While, M. V. Meissner, U. Wallrabe, and J. G. Korvink, “Magnetic Lenz lenses improve the limit-of-detection in nuclear magnetic resonance”, *PLoS ONE* **12**(8), e0182779 (2017). https://doi.org/10.1371/journal.pone.0182779

[6] K. Kitagawa, H. Gotou, T. Yagi, A. Yamada, T. Matsumoto, Y. Uwatoko, and M. Takigawa, “Space Efficient Opposed-Anvil High-Pressure Cell and Its Application to Optical and NMR Measurements up to 9 GPa”, *J. Phys. Soc. Jpn.* **79**, 024001 (2010). https://doi.org/10.1143/JPSJ.79.024001

[7] W. W. Brey, A. S. Edison, R. E. Nast, J. R. Rocca, S. Saha, R. S. Withers, “Design, construction, and validation of a 1-mm triple-resonance high-temperature-superconducting probe for NMR”, *J. Magn. Reason.* **179**, 290-293 (2006). https://doi.org/10.1016/j.jmr.2005.12.008

[8] H.D.W. Hill, “Improved sensitivity of NMR spectroscopy probes by use of high-temperature superconductive detection coils”, *IEEE Trans. Appl. Supercond.* **7**, 3750-3755 (1997). https://doi.org/10.1109/77.622233

[9] Jun-Bo Yoon and C.T.-C. Nguyen, “A High-Q Tunable Micro-Mechanical Capacitor with Movable Dielectric for RF Applications”, *Technical Digest of the International Electron Devices Meeting,* 489–492 (2000). https://doi.org/10.1109/IEDM.2000.904362

[10] R. L. Borwick, P. A. Stupar, J. DeNatale, R. Anderson, C. Tsai, K. Garrett, and R. Erlandson, “A high Q, large tuning range MEMS capacitor for RF filter systems”, *J. Sens. Actuators A* **103**, 33-41 (2003). https://doi.org/10.1016/S0924-4247(02)00316-3

[11] P. Styles, N.F. Soffe, C.A. Scott, D.A. Crag, F. Row, D.J. White, and P.C.J. White, “A high-resolution NMR probe in which the coil and preamplifier are cooled with liquid helium”, *J. Magn. Reason.* **60**, 397-404 (1984). https://doi.org/10.1016/0022-2364(84)90050-7

[12] P. Styles, N. F. Soffe, and C. A. Scott, “An improved cryogenically cooled probe for high-resolution NMR”, *J. Magn. Reason*. **84**, 376-378 (1989). https://doi.org/10.1016/0022-2364(89)90383-1

[13] P. F. Flynn, D. L. Mattiello, H. D. W. Hill, and A. J. Wand, “Optimal Use of Cryogenic Probe Technology in NMR Studies of Proteins”, *J. Am. Chem. Soc.* **122**, 4823-4824 (2000). https://doi.org/10.1021/ja993743x

[14] T. Horiuchi, M. Takahashi, J. Kikuchi, S. Yokoyama, and H. Maeda, “Effect of dielectric properties of solvents on the quality factor for a beyond 900 MHz cryogenic probe model”, *J. Magn. Reason.* **174**, 34-42 (2005). https://doi.org/10.1016/j.jmr.2005.01.004

[15] H. Kovacs, D. Moskau, and M. Spraul, “Cryogenically cooled probes—a leap in NMR technology”, *Prog. Nucl. Magn. Reson. Spectrosc.* **46**, 131-155 (2005). https://doi.org/10.1016/j.pnmrs.2005.03.001

[16] M. W. Voehler, G. Collier, J. K. Young, M. P. Stone, and M. W. Germann, “Performance of cryogenic probes as a function of ionic strength and sample tube geometry”, *J. Magn. Reason.* **183**, 102-109 (2006). https://doi.org/10.1016/j.jmr.2006.08.002

[17] T. Mizuno, K. Hioka, K. Fujioka, and K. Takegoshi, “Development of a magic-angle spinning nuclear magnetic resonance probe with a cryogenic detection system for sensitivity enhancement”, *Rev. Sci. Instrum.* **79**, 044706 (2008). https://doi.org/10.1063/1.2912946

[18] T. Mizuno and K. Takegoshi, “Development of a cryogenic duplexer for solid-state nuclear magnetic resonance”, *Rev. Sci. Instrum.* **80**, 124702 (2009). https://doi.org/10.1063/1.3263908

[19] Y. Matsuki, S. Nakamura, F. Hobo, Y. Endo, H. Takahashi, H. Suematsu, and T. Fujiwara, “Cryogenic signal amplification combined with helium-temperature MAS DNP toward ultimate NMR sensitivity at high field conditions”, *J. Magn. Reason.* **335**, 107139 (2022). https://doi.org/10.1016/j.jmr.2021.107139

[20] T. Hirata, T. Okazaki, K. Obara, H. Yano, and O. Ishikawa, “Development of Cryogenic Enhancement-Mode Pseudomorphic High-Electron-Mobility Transistor Amplifier”, *J. Low Temp. Phys* **187**, 596–601 (2017). https://doi.org/10.1007/s10909-017-1763-5

[21] D.V. Camin, G. Pessina, E. Previtali, and G. Ranucci, “Low-noise preamplifiers for 1 K operation using gallium arsenide MESFETs of very low 1/*f* noise”, *Cryogenics* **29**, 857-862 (1989). https://doi.org/10.1016/0011-2275(89)90162-8

[22] U. Tarvydytė, V. Kalendra, G. Usevičius, J. O’Sullivan, A. Brookfield, A. M. Bowen, J. Banys, J. J.L. Morton, and M. Šimėnas, “Pushing the sensitivity boundaries of X-band EPR cryoprobe using a fast microwave switch”, J. Magn. Reson. Open **23**, 100196 (2025). https://doi.org/10.1016/j.jmro.2025.100196

[23] S. Gong, H. Shen, and N. S. Barker, “A cryogenic broadband DC contact RF MEMS switch”, *2009 IEEE MTT-S Int. Microwave Symp. Dig.*, 1225-1228, (2009). https://doi.org/10.1109/MWSYM.2009.5165924

[24] P. Bradley, E. Sorenson, D. Lauria, and L.-A. Liew, “Characterizing MEMS Switch Reliability for Cryogenic Applications such as Quantum Computing”, *IOP Conf. Ser.: Mater. Sci. Eng.* **1302**, 012027 (2024). https://doi.org/10.1088/1757-899X/1302/1/012027.

[25] C. Brown, A. S. Morris, A. I. Kingon, J. Krim, “Cryogenic Performance of RF MEMS Switch Contacts”, *J. Microelectromech. Syst.*, **17**, 6, 1460-1467 (2008).

[26] A. M. Clogston, V. Jaccarino, and Y. Yaeet, “Interpretation of Knight Shifts and Susceptibilities of Transition Metals: Platinum”, *Phys. Rev.* **134**, A650 (1964). https://doi.org/10.1103/PhysRev.134.A650

[27] H. Suzuki, E. Kobayashi, S. Abe, K. Matsumoto, I. Mukhamedshin, A. Egorov, and M. Tagirov, “NMR study of enriched ^{195}Pt metal”, *Physica B* **329-333**, 1101-1102 (2003). https://doi.org/10.1016/S0921-4526(02)02358-X

[28] L. E. Drain, “Nuclear magnetic resonance in platinum”, *J. Phys. Chem. Solids* **24**, 379-382 (1963). https://doi.org/10.1016/0022-3697(63)90196-3